Physics – Uspekhi **68** (7) 641 – 652 (2025)

REVIEWS OF TOPICAL PROBLEMS

PACS numbers: **07.78.+s,** 61.05.J–, 64.70.D–, 64.70.K–, 68.37.Og

INTERNATIONAL YEAR OF QUANTUM SCIENCE AND TECHNOLOGY

Structural dynamics of thin-film materials: achievements, problems, prospects

S.A. Aseyev, B.N. Mironov, D.G. Poydashev, E.A. Ryabov, Z. Li, A.A. Ischenko

DOI: https://doi.org/10.3367/UFNe.2024.12.039828

Contents

Abstract. The use of short photoelectron pulses has opened up the possibility of studying structural dynamics with high spatiotemporal resolution. Within the framework of this methodology, a pulsed electron beam formed due to the photoelectric effect provides probing of light-induced fast processes in matter at different moments in time. The integration of pico-femtosecond laser technology and electron optics in an experimental setup has proven to be extremely effective for observing the behavior of atomic-molecular structures at their natural scales in the spatiotemporal continuum. In imaging mode, this concept has led to the creation of 4D electron microscopy, and, in the electron diffraction mode, a unique opportunity has appeared to shoot atomic-molecular movies. The high sensitivity of the method in combination with relatively low radiation damage to the sample (in contrast to an X-ray free electron laser) has made it possible to study promising thin-film materials on compact setups in standard laboratories. The review examines the development of this scientific field from the study of nanosecond structural dynamics to femtosecond quantum tomography based on ultrafast electron diffraction.

Keywords: ultrafast electron microscopy and diffraction, dynamic processes, structural dynamics, atomic-molecular cinema, femtosecond time resolution, atomic spatial resolution, electron tomography

S.A. Aseyev [1,a], **B.N. Mironov** [1,b], **D.G. Poydashev** [1,2,c], **E.A. Ryabov** [1,d], **Z. Li** [3,4,5,e], **A.A. Ischenko** [6,f]

[1] Institute of Spectroscopy, Russian Academy of Sciences, ul. Fizicheskaya 5, 108840 Troitsk, Moscow, Russian Federation
[2] National Research University Higher School of Economics, ul. Myasnitskaya 20, 101000 Moscow, Russian Federation
[3] State Key Laboratory for Mesoscopic Physics and Collaborative Innovation Center of Quantum Matter, School of Physics, Peking University, Beijing 100871, China
[4] Collaborative Innovation Center of Extreme Optics, Shanxi University, Taiyuan, Shanxi 030006, China
[5] Peking University, Yangtze Delta Institute of Optoelectronics, Nantong, Jiangsu 226010, China
[6] MIREA — Russian Technological University, Institute of Fine Chemical Technologies named after M.V. Lomonosov, prosp. Vernadskogo 86, 119571 Moscow, Russian Federation
E-mail: [a] isanfemto@yandex.ru, [b] mironov@isan.troitsk.ru, [c] poydashev@isan.troitsk.ru, [d] ryabov@isan.troitsk.ru, [e] zheng.li@pku.edu.cn, [f] aischenko@yasenevo.ru

Received 18 October 2024, revised 6 December 2024
Uspekhi Fizicheskikh Nauk **195** (7) 681 – 694 (2025)
Translated by S.D. Danilov

Centenary of Louis de Broglie's hypothesis

The electron can no longer be conceived as a single, small granule of electricity; it must be associated with a wave.
Louis de Broglie

1. Introduction

One hundred years ago, in 1924, Louis Victor Pierre Raymond, seventh Duc de Broglie (French physicist and aristocrat), postulated the wave nature of electrons in his thesis, proposing that all matter possesses wave properties [1]. This hypothesis (known as the de Broglie hypothesis), is an example of wave-particle duality in quantum mechanics. De Broglie was awarded the Nobel Prize in Physics in 1929 for predicting of the wave nature of electrons, while even earlier, in 1927, C.J. Davisson and L.H. Germer demonstrated electron diffraction when electrons were fired at a nickel crystal target [2], which then become the basis for a highly sensitive method of studying the structure of solids and molecules in a gaseous phase.

Throughout its century-long history, electron diffraction and microscopy have remained powerful tools for studying the structure of matter that is predominantly at or close to equilibrium [3]. However, to obtain a full picture of a studied object, it is also important to explore its dynamic properties.

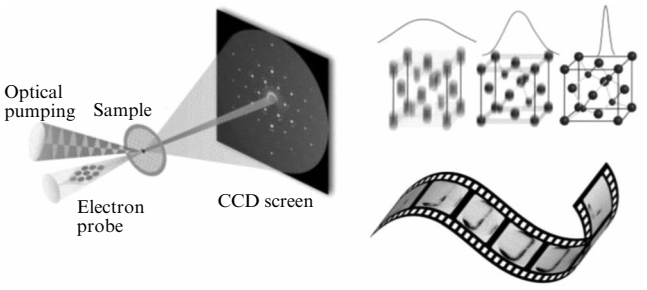

Figure 1. Concept of pulsed electron probe for imaging atomic motion in solids; if an electron packet interacts with a sample for a long time, this is accompanied by smearing of atoms as they move. When a probing electron pulse is sufficiently short, smear is minimal, ensuring sharp images of structure at a given time instant.

Time-resolved laser spectroscopy, based on a pulsed laser technique, has opened up the possibility of observing a wide range of rapidly evolving processes [4]. However, the potential of purely optical experiments is limited by their low spatial resolution, which highlights the need to develop diffraction methods.

Under the action of powerful laser pulses, matter is 'rearranged,' which is accompanied by a change in its structure. These structural dynamics are manifested in an atomic-molecular movie, the recording of which is of immense interest to fundamental science and applications alike [5]. In order to directly observe laser-induced structural changes, high spatiotemporal resolution is required above all else. Using ultrashort electron (or X-ray) pulses synchronized with 'optical triggering' of fast-evolving processes in a sample is key to solving this problem [5–9] (Fig. 1). Studying ultra-thin films and molecular-cluster ensembles benefits from using pulsed electron beams due to their higher interaction cross section with matter (up to 6 orders of magnitude greater than X-rays), a relatively low damage potential, and, importantly, the ability to perform measurements 'in dynamics' using compact laboratory setups [9].

In a pioneering experiment [10] carried out in Moscow in the 1980s, the structural dynamics of laser-induced dissociation of CF_3I molecules were observed. This process was detected by combining the high temporal resolution of a pulse laser with the subatomic spatial resolution of a gas phase electronograph. In what followed, this experiment predetermined the emergence of a new scientific discipline — Ultrafast Electron Diffraction (UED), and then Ultrafast Electron Microscopy (UEM). In these methods, short electron bunches, optically connected to a pulse master laser, probe a laser-excited sample at different time instants.

The appearance of reliable and affordable femtosecond (fs) lasers (predominantly solid-state systems based on titanium sapphire crystals) in scientific laboratories and the development of bright, technologically simple photoelectron pulse sources based on them led to a breakthrough in ultrafast electron diffraction [5–9]. As a result Miller et al. achieved a subfemtosecond temporal resolution [11], enabling the direct registration of atomic displacements in laser-stimulated chemical reactions using dense electron bunches with the UED method. This also facilitated the study of the correlation of a series of important structure functions that underpin chemistry and biology [5–9]. This work laid the foundation for femtosecond electron optics [12], which were initially applied to the regime of electron diffraction.

The imaging regime is important for studying spatially inhomogeneous structures, which greatly expands the range of problems that can be solved using electron beams. A quarter of a century ago, a scientific team led by Zewail (California Institute of Technology) conducted the first experiments using a modified transmission electron microscope, achieving a picosecond temporal resolution. The capabilities of the UEM were soon extended to the femtosecond temporal range, which was crucial for observing ultrafast structural dynamics on the natural spatiotemporal scales of the matter under investigation [6].

The development of transmission electron microscopy is inextricably linked to improvements in resolution [13]. While the capabilities of the first setups in the mid-20th century were comparable to the best optical microscopes, resolving microstructures with a characteristic size of 0.2 μm, electron optics now boast a resolution of about 0.07 nm, sufficient for the direct visualization of atoms [13, 14]. Thus, transmission electron microscopy (TEM), alongside an ion projector [15] and scanning probe microscopy [16], has become a highly accurate technique for observing the atomic and molecular structure of matter. Incorporating femtosecond and solid-state laser techniques into the TEM experimental scheme provided new momentum for the development of this technology [5–9].

A series of review articles and monographs devoted to the development of UED/UEM has been published recently. Reference [9] expands on the possibilities of shooting atomic-molecular movies with the help of bright sources of short electron pulses and surveys the history of UED development up to 2017. Book [17] presents the state of time-resolved electron microscopy in 2019, while Ref. [18] supplements these materials. Of note are the fundamental review of 2022 on the development of UED [19] and a relatively recent monograph [20] on the detection of structural dynamics using ultrashort electron and X-ray pulses.

The primary aim of this paper is to analyze publications on UED/UEM that were not covered or only touched upon in previous reviews. To demonstrate the potential of using short electron pulses for a structural analysis, we present a series of recent studies in this promising area of modern natural science.

2. Pulsed electron beam of short duration — basis of UED/UEM

The duration of electron pulses τ_e is a key parameter that largely defines the temporal resolution in UED/UEM. The concept of a femtosecond electron probe, when $\tau_e \leqslant 100$ fs, was first introduced in [21]. The photoeffect in a solid under the action of very short laser pulses proved to be an efficient basis for an electron source in UED and UEM, primarily due to the practically instantaneous response to the optical pulse. The lack of inertia in this process on a femtosecond timescale was experimentally demonstrated in [22].

An alternative to a solid state cathode can be the use of cold atoms. Subthreshold optical ionization of such a gas target can provide high spatial coherence of the probe in an experiment due to a practically 'zero' initial energy of free electrons [23]. Currently, success is being achieved in obtaining subpicosecond bunches as a result of two-step photoionization of a laser-cooled rubidium cloud [24]. While this complicates the experimental setup to some extent, it is promising for the study of biological molecules using the

UED/UEM method. An important parameter is the number of electrons in each bunch, which is generally defined by a compromise between 'how quickly' the measurement can be performed and 'how short' the detected process can be, since, unlike X-ray radiation, the electrons in the bunch experience Coulomb repulsion, which hampers temporal resolution.

Forming ultrashort multielectron pulses is an important task. In this context, it is relevant to consider the brightness of the electron probe in two limit cases: when observing diffraction and in the imaging regime. Let n represent the number of elementary cells in the part of crystal that is studied. Then, in electron diffraction observations, the signal is proportional to n^2; however, in the imaging regime, it is only proportional to n [9]. Therefore, in terms of measurement sensitivity, signal detection in the reciprocal space is preferrable.

Methods that allow high temporal resolution, reaching tens of fs, have been developed for dense probing pulses [9]. Two of these methods are particularly efficient. The first one uses a cell with an rf field to compress multielectron bunches. In this respect, it should be noted that it is possible to form spatially homogeneous pulses with an ellipsoidal shape for which the compression degree is maximal [25]. The problem of obtaining dense electron pulses in a nonrelativistic regime with $\tau_e \leqslant 100$ fs is explicitly illustrated in [26]. The second approach is the transition to relativistic velocities [27, 28]. The successful practical realization of these methods opens up the possibility of studying irreversible laser-induced processes with the help of UED [9]. There are recent indications of progress in applying such approaches to UEM based on transmission electron microscopy [20].

A simplified setup of an experiment in the field of UED/UEM (Fig. 2) is based on the pump-probe method and involves injecting laser emission into a column of an electronograph or a transmission electron microscope [29–34]. One channel is used to generate short electron bunches, which can be obtained, for example, through the photoeffect when a laser beam is shone on a solid-state cathode. The second channel corresponds to optical sample excitation. Precise synchronization of the channels is achieved by using the same master laser. The delay between exciting structural dynamics and probing them is determined by the optical path lengths. By varying these in the experiment, the process under study can be stacked in time. A position-sensitive detector records signal frames at each time step.

When the studied sample is illuminated by a high-intensity laser pulse, the observed diffraction pattern varies according to the Debye–Waller factor due to thermal oscillations of the atoms in the crystal lattice (Fig. 2). In the theoretical framework, a particular area of scientific interest is the calculation of this factor for complex multi-atomic systems, for which knowledge of the dispersion law of the medium is strictly necessary, as is a rigorous account of the influence of multi-photon effects, which presents quite an intricate problem. Such an analysis can be substantially simplified for ultrashort electromagnetic pulses [35].

As the thawing of glaciers informs developments in modern Earth climate theory, a reduction in the strength of electron beam scattering by a crystal, which leads to a decrease in the height of diffraction peaks (as the temperature of the crystalline lattice increases), allows important conclusions to be drawn about energy transport in solids on the nanoscale. The authors of Ref. [36] detected deviations from the known two-temperature model, which describes the

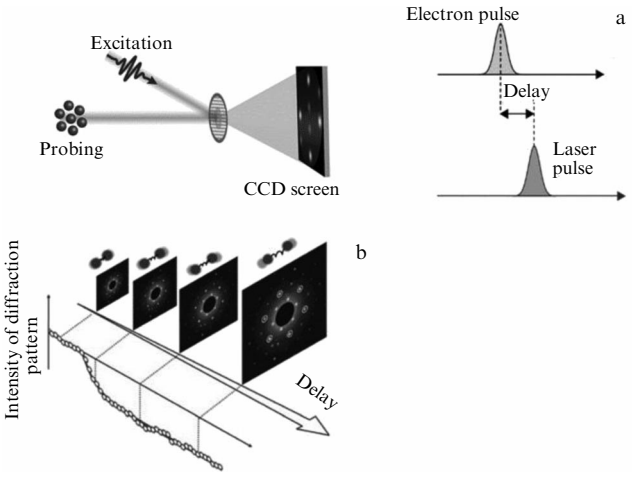

Figure 2. (a) Schematic of excitation–probing of structural dynamics based on short electron pulses; (b) recording frames of diffraction pattern at different moments of time with UED method.

dynamics of the excitation of electron and phonon subsystems in condensed media, using the UED method and a thin crystal of Al [37, 38]. Furthermore, a thorough analysis of diffraction patterns obtained from a laser-excited sample by capturing images with the help of short electron pulses at different time moments allows one to identify the initial stage of nonthermal melting in a substance, i.e., in a thin bismuth crystal [39]. A key aspect of the successful experiment in this case was achieving a sufficiently low level of transient fluctuations in the photoelectron beam, which presents certain technical difficulties.

An adapted transmission electron microscope enables the study of irreversible, light-induced phenomena on a nanosecond timescale in the regime of a single pulse containing up to $\sim 10^8$ electrons, and strictly reversible processes due to the accumulation of a large number of 'rarefied' electron bunches ($\sim 10^3\,e^-$), providing high spatiotemporal resolution by suppressing Coulomb repulsion [3, 6]. The development of a stroboscopic method to record dynamical effects in TEM dates back to the 20th century [40, 41]. The method involves probing a sample (with periodically varying properties) using electron pulses of the same frequency and a fixed phase. (Note that a picosecond temporal resolution can currently be achieved without using the pulsed laser technique [42].) Using laser sources of ultrashort pulses has fostered rapid progress in developing this method. The first TEM adapted for studies of ultrafast laser-induced processes was created at the California Institute of Technology [8].

4D electron microscopy detects structural dynamics within a spatiotemporal continuum by combining the capabilities of an electron microscope and a pulsed laser. Inelastic interactions between electrons and photons in the presence of a nanostructure can result in changes in the probe energy [43–45]. In Photon-Induced Near-Field Electron Microscopy (PINEM), an intense laser field propels an electron into a superposition of quantum mechanical states. For the initial electron energy E_0, the interaction of the electron with an incident light wave then broadens the energy spectrum by populating new energy states (known as sidebands), which are separated from E_0 by intervals that are multiples of the photon energy $\hbar\omega$. Analysis of kinetic energy using Electron Energy Loss Spectroscopy (EELS) in TEM extends the range of problems that can be solved using UEM [44].

Previously, collective plasmon resonances in solids could only be studied using transmission electron microscopes under stationary conditions. This ruled out the observation of fast transient processes in real time. Ultrafast optical spectroscopy was also unable to provide an acceptable spatial resolution due to the diffraction limit. Reference [41] uses PINEM in an adapted TEM column to explore the behavior of light-induced plasmons with an energy resolution of 20 meV, defined solely by the width of the laser line. The development of a new 5D UEM method [45, 46] has opened up the possibility of reaching a spatiotemporal continuum, augmented with the energy resolution.

Unlike traditional methods of inelastic scattering, the resolution of the 5D UEM method is determined solely by the spectral properties of laser excitation and is not limited by the energy spread of fast electrons [46]. This is of particular interest to photonics and plasmonics, as the ability to generate monochromatic laser light with a controlled temporal profile has a broader range of applications than classical electron optics does. This includes the study of practically any low-energy mode in solids, provided it can be selectively optically excited. By measuring the spatiotemporal and spectral profiles of coherent phonons, it is possible not only to study the connection between the lattice and electron subsystem in real time but also to develop a method to control the dynamics of prospective materials. Combining 5D UEM with the method of selective population of oscillatory states in catalyzers based on plasmonic nanostructures makes it possible to visualize the course of chemical reactions [46].

Three types of cathodes are used in classical TEM: (1) a cathode based on thermionic emission; (2) a Schottky emitter, where the thermionic emission is amplified in a strong electric field; (3) a cold-field point emitter, which does not require heating. When adaptating the microscope, it is important to consider that it is problematic to achieve an acceptable brightness of electron pulses for a flat photocathode due to the relatively large initial size of the electron source, which is defined by the laser beam diameter.

Using a point cathode provides a solution to this problem, as the 'locally compressed' emission minimizes the volume of phase space occupied by photoelectrons, ensuring their high coherence. In one of the first demonstrations, the probe was formed using emission from a Schottky cathode [47]. In this experiment, a 100-nm ZrO/W needle was illuminated by the second harmonic of a fs Ti:Sa laser ($\lambda = 400$ nm, $\hbar\omega = 3.1$ eV). In a strong electric field with a strength of ~ 1 V nm^{-1}, the work function was reduced to 2.9 eV, providing a condition for a linear photoeffect. Consequently, the diameter of the probe on the sample could reach 9 Å for the duration of pulses of 200 fs with a repetition frequency f up to 800 kHz and transverse coherence of 1.2 μm, which is sufficient to study complex biological structures.

In [48], a cold-field emitter of electrons was used for nonlocal photoemission. In this case, a 100-nm tungsten needle in TEM was illuminated by the second harmonic of the fs fiber laser ($\lambda = 515$ nm) in the multi-photon electron emission regime. An important feature of the fs fiber laser is the high frequency of the pulse sequence, which can be varied relatively easily in experiments. As a result, 20-electron pulses were formed with f up to 1 MHz and a kinetic energy up to 200 keV, enabling precise experiments in electron holography. It should be noted that the duration of such electron pulses is practically unaffected by Coulomb repulsion, creating unique possibilities for studying reversible fast transient processes with a high spatiotemporal resolution.

Reference [49] demonstrated the production of holograms through the scattering of a pulsed electron beam in a strong laser field. This has actually become the first experimental realization of Gabor's original idea, aimed at improving the transmission electron microscope, but initially developed in optics. The well-known principle of holography involves recording the amplitude-phase characteristics of a signal by mixing it with a known reference signal. In [49], an adapted transmission electron microscope was used to achieve an ultrahigh (in perspective, attosecond) temporal resolution in combination with a nanometer spatial resolution when creating holograms of local electromagnetic fields. Unlike the 'classical method,' where the signal and reference fields are initially spatially separated and then are mixed to form an interference pattern (a hologram), in [49], the electromagnetic fields split the electron wave function into a quantum-coherent superposition of different energetic states. As a result, the spatial modulation of the electron energy distribution reflects the phase relationship between the reference and signal fields. Overcoming the femtosecond barrier and exploring the attosecond time range are promising areas for future research.

3. Development of structural dynamics detection methods using electron pulses and exploration of femto-attosecond range

Recent work at the Massachusetts Institute of Technology (MIT) has confirmed that a pulsed electron beam can be used to take precise measurements of comparatively small laser-induced structural changes in a sample. The success of this approach is largely due to the use of high-quality crystal films as samples [50]. Reference [51] explores a gigahertz structural resonance in a 16-nm antiferromagnetic film ($FePS_3$) when the material is cooled below the Néel temperature. Using the UED method, a shift in the layers of the sample is recorded when an electron beam with a kinetic energy of 28 keV is used to illuminate the sample. This causes individual regions of the thin antiferromagnetic film to displace parallel to each other, in a manner similar to coherent oscillators.

Thorough studies of two-dimensional (2D) crystals open up new functional possibilities in material science. In this class, freestanding films have emerged as a universal platform for designing 2D materials due to their unique properties, which are not found in flat structures on a substrate. A characteristic example is the dynamics of wrinkles, which has not been studied in much detail. In [52], laser-induced structural changes in a freestanding film of $La_{2/3}Ca_{1/3}MnO_3$ were directly observed. Analysis of diffraction peaks helped to qualitatively reconstruct the dynamics of wrinkle formation on a picosecond timescale. It was found that this process is associated with a relatively fast delamination of the sample at the contact (tangent) point between the film boundary and the support. This result confirms the importance of considering the interaction between the film and its surroundings, even for freestanding structures.

The success of the experimental work described is at least partly due to the use of high-quality, thin, homogeneous crystal films of a large lateral size as samples. One of the main factors that complicates the analysis of the diffraction pattern is the need to use a dynamical scattering theory [53], which, strictly speaking, should be considered even for very thin

samples (for example, for a 40-nm gold film) and subrelativistic velocities (energy of 750 keV) of the probing electrons [54].

Due to the strong elastic and inelastic scattering of electrons in solids, the kinematic theory (Born's approximation of the scattered wave being much weaker than the incident wave) is, strictly speaking, applicable only to very thin samples. For 'thick' crystals, the dynamical theory must account for the interaction between the primary and diffraction beams. In this case, multiple scattering of electrons can redistribute the intensity between different Bragg peaks. According to witnesses, there were attempts to involve L.D. Landau in developing the dynamical scattering theory in the middle of the last century (but they were unsuccessful).

The use of the kinematic approximation in the analysis of diffraction patterns is more appropriate for molecular ensembles in a gas phase. Some progress is currently being achieved in the field of a gas UED. In [55], the dynamics of rehybridization in an electrocyclic reaction were observed using a relativistic electron beam ($\sim 3 \times 10^4\,e^-$ in a pulse) with a kinetic energy of 4.2 MeV. Electron bunch compression was achieved using an rf field, enabling temporal resolution on the level of several hundred fs.

It is known that reactions of this type are characterized by the concerted formation and breakup of σ- as well as π-bonds in a pericyclic transient state. Therefore, observing the structural dynamics of such a state in real time is of great interest in both practical and fundamental aspects. To address this significant issue, molecules of α-terpinene ($C_{10}H_{16}$) were used as an example and a combination of UED (experiment) and modeling of wave packets in an excited state (theory) was applied in [55]. Upon reaching a pericyclic minimum in this molecular complex, it was found that the rehybridization of two carbon atoms was dominant, ensuring the transformation from two to three conjugate π-bonds, while the dissociation of the σ-bond predominantly occurred after conversion from the pericyclic minimum to the electron ground state. The findings obtained in [55] can be generalized to electrocyclic photochemical reactions in general.

Hydrogen is a component of many substances. However, observing structural dynamics involving H atoms is difficult due to their low scattering cross section. To address this issue, the UED method using a 4.2-MeV electron beam was employed in [56]. The high sensitivity of this approach is demonstrated using the example of laser-induced dissociation of gaseous ammonium. In this study, the measurements of nuclear and electron dynamics in gas molecules were *ab initio* augmented by modeling. Although the 500 fs resolution was insufficient to study the dissociation process in detail, the results obtained in [56] present a significant advance in the observation of proton dynamics in space and time.

Solving the ill-posed inverse problem is a distinguishing feature of the diffraction approach, but it is linked with certain conceptual difficulties. Studying spatially inhomogeneous structures and the influence of local irregularities on dynamics requires special methods. Therefore, observations of structural dynamics in the imaging regime are important and can be realized with the help of TEM. Ultrafast electron microscopy can provide new insights into the optical excitation process [43–46].

The electrodynamic response of electrons to an incident electromagnetic wave forms the basis of practically any interaction between light and matter. Therefore, a thorough

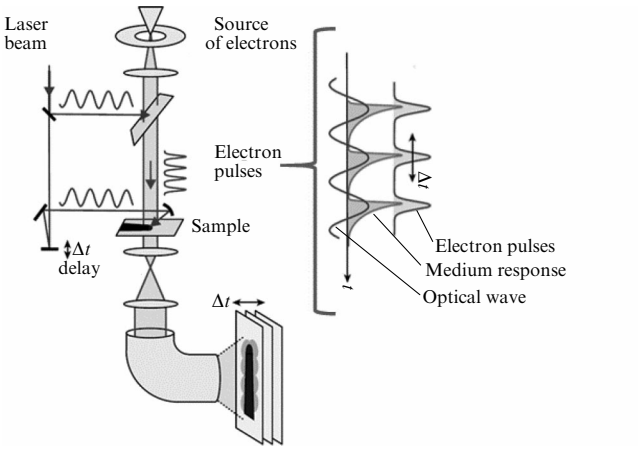

Figure 3. Attosecond UEM. Continuous laser illuminates thin membrane and sample. Subfemtosecond electron pulses probe the sample; change in kinetic energy of transmitted electrons is detected by EELS spectrometer. Temporal synchronization in this approach is illustrated on right.

study of this process at sub-wave (in space) and sub-cycle (in time) scales is essential for modern optics and nanophotonics. Although the short length of the de Broglie wave for free electrons (e.g., in TEM) in principle allows access to attosecond/angström scales, the temporal resolution of UED/UEM has thus far been limited to the femtosecond range at best, which is apparently insufficient for solving such fundamental problems. Reference [57] demonstrated an efficient approach that circumvents these difficulties. An adapted transmission electron microscope equipped with a field Schottky emitter, with an electron energy of 183 keV, was used as an instrument (see Fig. 3). In the experiment, a sample (a sharp tungsten needle) was excited by a continuous laser ($\lambda = 1064$ nm) and probed by a train of ultrashort electron bunches. This involved converting a continuous electron beam into a sequence of attosecond pulses through the periodic modulation of the wave function (of free electrons) using optical electric fields, which was achieved as the electrons passed through a very thin 200-nm silicon membrane illuminated by a laser (Fig. 3). In the experiment in [57], changes in electron energy at different instants of time, as set by the delay line, were detected using an electron spectrometer. In the EELS regime, a special filter can be used to detect sidebands (which correspond to discrete changes in kinetic energy), allowing accurate measurement of the sample's near field response in the spatiotemporal continuum.

Indeed, the electron wave function remains intact for more than one period of an optical cycle (several fs), which, in principle, allows detecting coherent sidebands. Since fast electrons pass through the 200-nm interval in a subfemtosecond time, the electromagnetic fields inside and on the surface of the sample appear to be practically frozen with regard to probing. In particular, the longitudinal modes, which correspond to the optical excitation of the tungsten needle, can coherently change the kinetic energy of the electrons in the probing beam, which is reflected in the detected EELS spectrum.

Thus, UEM enables precise measurements of the near field in the spatiotemporal continuum [57]. In experiments involving conducting tips, dielectric resonators, and antennas based on metamaterials, directional excitation of chiral

surface waves was detected, and the lag between the dipole and quadruple dynamics was found as well. These results demonstrate the power of the UEM, which is particularly important for understanding light-matter interactions within the context of fundamental research into their spatiotemporal properties [57, 58].

In [59], PINEM was applied to study soliton formation in optical integral schemes. The interaction between an electron and a soliton is accompanied by a change in electron distribution, opening up a new area of UEM. Shortly after the initial PINEM studies, an important coherence relationship was established between various electron waves corresponding to different sidebands [43–45]. As the sidebands (with different energies) are characterized by different electron velocities, the shape of the related wave packet, which is their superposition, changes in space and time as the packet propagates. Ultimately, the probe can become a train of very short pulses, which, in principle, allows a significant increase in electron microscope resolution. The amplitude corresponding to the sideband also characterizes the near optical field through which the electron passes. This effect is used to study Kerr solitons in a silicon nitride microresonator with a diameter of hundreds of micrometers in [59].

In principle, successful realization of PINEM requires rather intense optical fields, which are commonly generated using powerful laser pulses. However, these conditions can also be obtained using an optical microresonator — specifically, a waveguide fabricated from a transparent silicon nitride on a silicon chip using lithography [59]. After light is directed into the closed structure, it circulates many times within a ring-shaped cavity, and in this way enables PINEM with the help of a continuous-wave laser.

Silicon nitride exhibits a strong nonlinear optical response. As a result, the speed of light in Si_3N_4 depends on the intensity of the electromagnetic field, even for a moderate laser power. Above a certain threshold, the nonlinearity causes light to propagate in a complicated way, including, for example, the formation of Kerr solitons. In order to excite these solitons, silicon nitride was illuminated by a continuous-wave laser with wavelength $\lambda = 1.55$ μm, which is typically employed in telecommunications [59]. In the experiment (Fig. 4), the TEM axis and the microresonator are aligned so that a free electron can interact with the sample twice, probing the electromagnetic field in the ring at two different times, with the lag between them being controlled by the probe displacement from the cavity center. Studying the propagation of light waves in this way enabled the observation of characteristic Ramsey-type interference.

The soliton signature superimposed on the Ramsey diagram was manifested in higher-order sidebands. Depending on the laser power, it turned out that it is possible to observe chaotic light fields or trains of solitons in such conditions (Fig. 4). The ability to study transitions between different nonlinear optical regimes is in practice due to the high sensitivity of PINEM to the light field intensity and distribution in the ring.

The results of [59] can be explained using known theoretical models that describe the nonlinear optical response of microresonators in the context of electron-photon interaction. These studies pave the way for obtaining information on light propagation inside integral optical schemes, which was previously inaccessible and has significant implications. Solitons cycling in a closed cavity can

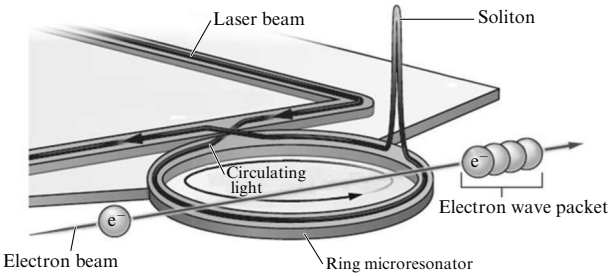

Figure 4. Electron beam in TEM, combined with ring microresonator, probes ultrafast evolution of optical solitons created in ring by continuous laser light. Strong electron-photon interaction provides formation of ultrashort electron pulses with 'slightly' modified kinetic energy (change in kinetic energy of electrons is registered by EELS spectrometer).

interact effectively with a continuous electron beam at a high repetition frequency approaching the terahertz level, which is still beyond the reach of existing optical modulation methods. Meanwhile, electron modulation in TEM, synchronized with laser excitation, could form the basis of powerful methods for observing the dynamics with a spatiotemporal resolution better than fs nm^{-1}.

In studies of the structure of protein complexes with high spatial resolution, up to the atomic level, particular attention is currently being paid to conformational dynamics [59]. However, most experiments in this area were previously performed using a laser on free electrons, in the regime of sequential femtosecond crystallography [60], which presented certain difficulties (the use of large-sized setups and possible sample damage by X-rays). One of significant advantages of using electrons as opposed to X-rays in time-resolved diffraction is that a useful scattering event requires fewer and smaller protein crystals.

Reference [32] provides a detailed analysis of two promising methods that gained popularity recently: electron microdiffraction and ultrafast electron microscopy (Fig. 5). Using electron pulses to study protein crystals has already been shown to be an efficient way of measuring intermolecular forces in such materials. Experiments of this kind have been shown to be possible with sufficiently low doses of pulsed photocurrent in a transmission electron microscope column, due to the relatively high interaction cross section of electrons with matter and the use of high-sensitivity detectors.

The authors of [32] analyzed the main difficulties in collecting and processing data, paying particular attention to the signal-to-noise ratio. They describe the efficiency of the working process for a minimum admissible dose of a photoelectron beam in detail. They also present a set of model samples as candidates for test measurements. Thus, using an adapted transmission electron microscope to observe laser-simulated processes in biological molecules has moved into the practical domain.

The combination of microED and UEM offers unique opportunities to study the structural dynamics of protein complexes. As earlier work on time-resolved electron diffraction of organic microcrystals found, spatial resolution can be better than 3 Å even when subject to Coulomb repulsion in the microscope column. This is highly promising for a complete understanding of the laser-induced dynamics of complex molecular systems over time scales ranging from micro- to sub-pico-seconds, and possibly even shorter.

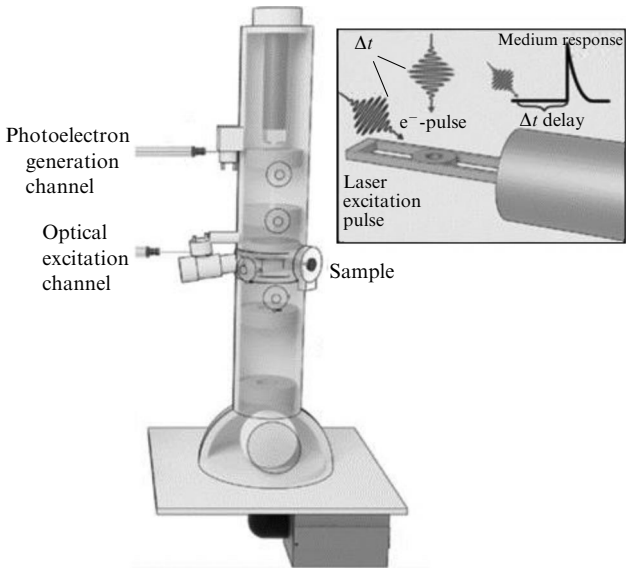

Figure 5. Schematic of ultrafast transmission electron microscopy (UEM).

4. Prospects for detecting structural dynamics of ion channels

The development of microfocus stations based on synchrotrons and the emergence of free electron X-ray lasers have made serial crystallography a working tool for studying membrane proteins in structural biology. Within this methodology, a diffractogram (X-ray image) of a biological microcrystal at room temperature is formed in less time than it takes for radiative sample damage to occur, ensuring an effective collection of structural information about the protein being studied. The use of powerful, focused X-ray pulses (with a characteristic focal spot size of ~ 10 nm and pulse duration of about ~ 10 fs) creates unique opportunities for studying biological structures. One of the main difficulties in structural biology is preparing samples to be probed. Membrane proteins tend to form very small crystals, resulting in a substantially worse quality of diffraction patterns than those obtained from soluble proteins samples. Using a technique known as the lipid cubic phase (LCP) has been shown to be a convenient way to solve this problem [61]. As a result, serial femtosecond crystallography (SFC) has became widely adopted thanks to special injectors for viscous solutions of membrane proteins. In SFC, X-ray patterns are registered for an ensemble of microcrystals in the LCP, with only one image recorded per crystal. Then, the entire array of experimental data is combined into a single array [62, 63].

In structural biology, the light-induced isometrization of retinal in bacteriorhodopsin (bR) is considered to be one of the fastest reactions. The development of the SFC method has made it possible to study the photochemical reaction in this protein with femtosecond and atomic resolution in time and space, respectively. For reference, bacteriorhodopsin is a membrane light-sensitive protein that, like chlorophyll, converts solar light energy into the energy of chemical bonds and in fact acts as a light-induced proton pump. Absorption of a photon is accompanied by a practically instantaneous change in the protein structure, facilitating the transfer of a proton from the cytoplasm to the outer side of the cellular membrane. In photoisomerization, the chromophore (retinal), which is attached to the inside of a bundle of spirals and closes the central channel of bR, changes from the full-*trans*-state into 13-*cys*-form. During photoinduced bending, the retinal carries a proton from one end of the semi-spiral bundle to the other.

A rather low scattering cross section of X-rays in matter means that 'thick' samples must be used in experiments, which presents a certain problem for optical excitation of laser-induced dynamics. Indeed, due to the absorption of a low-intensity laser beam, structural dynamics are confined to the near-wall layer, while multi-photon processes begin to dominate when the optical excitation power is increased [64], which does not correspond to the biological function of the protein [65, 66].

An important advantage of probing a biological sample with a pulsed electron beam compared to X-rays is the ability to provide a practically uniform optical excitation of the sample volume (initiating structural dynamics) with a relatively low level of radiative damage and in a compact experimental setup. Such studies will be possible in the very near future [67].

5. Femtosecond quantum tomography: on the way to quantum limit

Quantum tomography (QT) is widely used in many areas, including quantum optics [68–70], quantum computation [71, 72], and quantum information [73, 74]. In 1933, Pauli formulated the QT problem for a pure quantum state $\psi(x)$ in one dimension. Can the measurement of the time-evolving probability density $\Pr(x,t) = |\psi(x,t)|^2$ be used to determine the quantum state $\psi(x,t)$? According [75, 76], the absolute value of the wave function $|\psi(x,t)|$ can be obtained directly from $\Pr(x,t)$, and the phase can be recovered by measuring $\Pr(x,t)$ at certain points in time. This method has been extended to general one-dimensional quantum states, which are fully described by their density matrices $\hat{\rho}$, or, equivalently, their Wigner functions $W(x,p)$ [77], defined as

$$W(x,p) = \frac{1}{\pi\hbar}\int \mathrm{d}x' \langle x + x'|\hat{\rho}|x - x'\rangle \exp\left(\frac{\mathrm{i}2px'}{\hbar}\right). \quad (1)$$

$W(x,p)$ represents the distribution of quasi-probability in phase space, and the probability density is

$$\Pr(x) = \int \mathrm{d}p\, W(x,p)\,.$$

The inverse Radon transform is used for phase space tomography [78, 79].

Consider the case of a one-dimensional harmonic oscillator. The time evolution of the position x and momentum p in phase space represents circular motion,

$$x_\theta = x\cos\theta + p\sin\theta\,, \quad p_\theta = -x\sin\theta + p\cos\theta\,,$$

where $\theta = \omega t$ is the rotation angle, and ω is the frequency of the harmonic oscillator. By analogy with computer tomography, if the integral projection of the Wigner function along each rotated axis p_θ is measured,

$$\Pr_\theta(x) = \int \mathrm{d}p\, W(x_\theta, p_\theta)\,, \quad (2)$$

the Wigner function can be recovered using the inverse Radon transform [79, 80]

$$W(x,p) = -\mathbf{P}\frac{1}{2\pi^2\hbar}\int \mathrm{d}x' \int \mathrm{d}\theta \frac{\Pr_\theta(x')}{(x\cos\theta + p\sin\theta - x')^2}\,, \quad (3)$$

where **P** is the Cauchy principal value. In addition to the potential of the harmonic oscillator, it was shown that the full quantum state can be recovered for an arbitrary bounded potential $U(x)$ by measuring the motion of wave packets [81]. The initial density matrix in the basis of eigenstates $\psi_n(x)$ is ρ_{mn}, and the time evolution of the probability density is expressed as follows:

$$\Pr(x,t) = \sum_{mn} \rho_{mn}\psi_m(x)\psi_n(x)\,\exp\left[-\mathrm{i}\,(\omega_m-\omega_n)t\right], \quad (4)$$

where $\psi_n(x)$ is the eigenstate with eigenfrequency ω_n. The components of the density matrix can be obtained from the measured $\Pr(x,t)$ with the help of [81],

$$\rho_{mn} = \int \mathrm{d}x\,\widetilde{\Pr}(x,\omega_m-\omega_n)\,\frac{\partial}{\partial x}\left[\psi_m(x)\phi_n(x)\right], \quad (5)$$

where $\widetilde{\Pr}(x,\omega)$ is the Fourier transform of $\Pr(x,t)$, and $\phi_n(x)$ is the nth nonregular eigenstate of the Schrödinger equation [82].

There are many theoretical [78, 83–86] and experimental [87–89] studies of tomographic reconstruction methods and their applications to various systems. For instance, the quantum state of free electrons can be reconstructed using ultrafast transmission electron microscopy [69]. The Wigner function of a dissociating molecule of I_2 is determined by probing the distribution of the positions and velocities of the atomic fragments [90]. The degree of freedom of the mass center of He is found using diffraction patterns with temporal resolution [91]. The oscillatory wave packet of the dimer of Na_2 can be recovered from time-dependent fluorescence spectrum measurements [89]. The appearance of ultrafast electron and X-ray diffraction methods [92–97] has sparked significant interest in studying nuclear motions and creating 'molecular movies.' Combining observables from ultrafast diffraction visualization and quantum tomography opens up new possibilities for visualizing molecular wave functions and retrieving full information about the quantum state. However, the problem of dimensionality [78, 83, 84] seriously limits the application of traditional QT methods, and QT cannot be applied to all rotational and the majority of oscillatory wave packets in molecules.

Traditional QT methods use integral transformations, such as the inverse Radon transform, to reconstruct the density matrix from the probability density of a wave packet. Consider a molecular oscillatory wave packet. The probability density $\Pr(x_1,x_2,\ldots,x_N,t)$ is $(N+1)$-dimensional, where N is the number of oscillatory modes. The dimension of its density matrix is $2N$, and traditional QT methods can only be applied for one-dimensional oscillatory motions, since the integral transforms preserve dimension [78]. Similar problems exist for rotational states. For a linear rotor, the probability density $\Pr(\theta,\phi,t)$ is three-dimensional, while the density matrix is four-dimensional.

The dimensionality problem in QT can be solved by adding extra information to compensate for the additional dimension when reconstructing the density matrix from the time-evolving probability density. Analogous to crystallographic phase retrieval (CPR) [98, 99], to recover phase information of form factors $f(s)$ from the intensity of diffraction $I(s) = |f(s)|^2$, the transformation between the electron density in real space, and the form factor in the Fourier space is performed iteratively to impose physical constraints in both spaces [100–102].

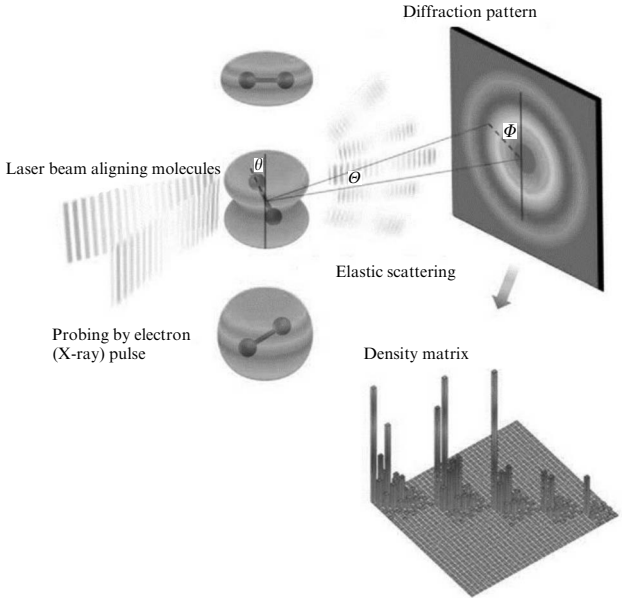

Figure 6. Schematic of quantum tomography of state of molecular rotational wave packet using ultrafast diffraction. Rotational wave packet of N_2 molecules is prepared by a pulsed aligning laser action and probed by ultrafast electron diffraction. Density matrix of rotational wave packet of N_2 is recovered from diffraction pattern [103].

The iterative projection method transforms the density matrix space in the probability density space. It is used for QT of a rotational wave packet of laser-aligned N_2 molecules, as shown in Fig. 6 [103].

Additional information includes the physical constraints of the density matrix space, such as its positive semidefiniteness and Hermitian character, as well as the selection rules of the prepared initial state. This method can be directly generalized to the quantum mechanics for high-dimensional oscillations [103], as well as to other systems where incomplete measurements provide only limited information about the quantum state (Fig. 7).

Having discussed QT for rotational and oscillatory wave packages, it is natural to generalize QT by including electron degrees of freedom (DOFs), thereby reconstructing full information about the quantum state of molecules. However, the dynamics of the electron state are strongly coupled with nuclear motion, and this interaction leads to fundamental differences in QT calculations for nuclear and electron degrees of freedom. When considering QT for an individual DOF, such as oscillation or rotation, we use quantum-state tomography (QST), in which the temporal resolution $\rho_{mn}(t)$ is known. In the basis of rotational and oscillatory eigenstates, the density matrix only includes the evolution of the dynamic phase factor

$$\rho_{mn}(t) = \rho_{mn}(0)\,\exp\left[-\mathrm{i}\,(\omega_m-\omega_n)t\right].$$

In QST, the temporal evolution of $\rho_{mn}(t)$ is known; therefore, measurements taken at different times provide additional information that can be used to recover the phase of the wave function [76].

The strong coupling between the electrons and nuclei plays a role of interaction system–surrounding medium, so that the temporal evolution of the reduced density matrices for nuclear or electron degrees of freedom is nontrivially dominated by the Hamiltonian of the nuclear or electron

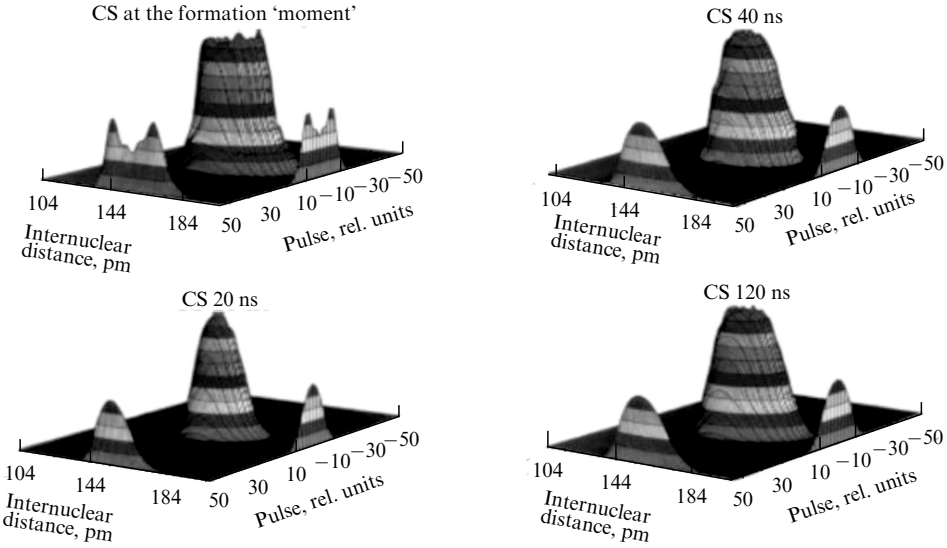

Figure 7. Wigner function of CS molecule. For initial distribution ($\sim$ 1 ps), Wigner function was found using full density matrix obtained in QT calculations. Wigner functions for different time delays (τ_d = ns, 40 ns, and 120 ns) were obtained by tomographic reconstruction which used procedure described in [104].

degrees of freedom. Therefore, the entire temporal evolution of the density matrix must be reconstructed at each instant of time. Pioneering work revealing the connection between electrons and nuclei and nuclear motion using QST was based on the dynamics of photodissociation of CS_2 excited by a 193-nm laser, which predominantly proceeds along two channels [104]:

$$CS_2\,(^1B_2) \rightarrow CS\,(X^1\Sigma_g^+) + S\,(^3P_J)\,, \tag{6}$$

$$CS_2\,(^1B_2) \rightarrow CS\,(X^1\Sigma_g^+) + S\,(^1D_J)\,. \tag{7}$$

Based on electron time-resolved diffraction data, the probability distribution of the distance between CS nuclei is measured for different time intervals to reconstruct the Wigner distribution function for various time delays τ_d [80]. As shown in Fig. 7, the system moves to an equilibrium state due to intermolecular oscillatory energy transfer during the first 20 ns, while the bimodal Wigner distribution evolves into a narrower unimodal one. Between 20 and 40 ns, the change in the Wigner function is caused by processes involving electron oscillatory energy transfer through collisions between S atoms and CS molecules [80].

QT of the reduced density matrix in the electron state basis can be used to reconstruct the time evolution of populations and coherences. Consider the wave function

$$\Psi(\mathbf{r},\mathbf{R},t) = \phi_g(\mathbf{r};\mathbf{R})\,\psi_g(\mathbf{R},t) + \phi_e(\mathbf{r};\mathbf{R})\,\psi_e(\mathbf{R},t)\,, \tag{8}$$

where $\mathbf{r}$ and $\mathbf{R}$ are the electron and nuclear coordinates, ϕ_g and ϕ_e are the main and excited electron state, and ψ_g and ψ_e are the related nuclear wave packets in each electron state.

The reduced density matrix in the electron state basis is

$$\rho_{ab}(t) = \int \mathrm{d}\mathbf{R}\,\psi_a^*(\mathbf{R},t)\,\psi_b(\mathbf{R},t)\;\;(a,b = \mathrm{g},\mathrm{e})\,, \tag{9}$$

where ρ_{gg} and ρ_{ee} are the populations in the ground and excited states, and ρ_{eg} is the coherence. The nuclear wave packets ψ_g and ψ_e move along surfaces of the potential energy of the ground and excited states and their crossing integral defines ρ_{eg}. In contrast to QST, it is necessary to reconstruct the temporal evolution of $\rho_{ab}(t)$, reflecting the transition of population and the dynamics of coherence of the coupled nuclear and electron degrees of freedom.

Ultrafast X-ray and electron diffraction visualization encodes the information about the electron state density matrix $\rho_{ab}(t)$. The total diffraction signal for the wave function $\Psi(\mathbf{r},\mathbf{R})$ in equation (8), including both the elastic and inelastic parts, is [105–108]

$$I(s,t) = \sum_{ab}\int \mathrm{d}\mathbf{R}\,\psi_a^*(\mathbf{R},t)\,I_{a,b}(\mathbf{R},\mathbf{s})\,\psi_b(\mathbf{R},t)\,, \tag{10}$$

$$I_{a,b}(\mathbf{R},\mathbf{s}) = \int \mathrm{d}r\,\phi_a^*(\mathbf{r};\mathbf{R})\,\hat{\sigma}^\dagger\hat{\sigma}\,\phi_b(\mathbf{r};\mathbf{R})\,, \tag{11}$$

where $\mathbf{s}$ is the vector of momentum transfer of the incident X-ray or electron, and $\hat{\sigma}$ is the scattering operator.

The scattering operators for the diffraction of X-rays and electrons are [109, 110]

$$\hat{\sigma}_X = \sum_j \exp\left(\mathrm{i}\,\mathbf{s}\mathbf{r}_j\right), \tag{12}$$

$$\hat{\sigma}_e = \frac{1}{s^2}\left[\sum_v N_v \exp\left(\mathrm{i}\,\mathbf{s}\mathbf{R}_v\right) - \sum_j \exp\left(\mathrm{i}\,\mathbf{s}\mathbf{r}_j\right)\right], \tag{13}$$

where $\mathbf{r}_j$ and $\mathbf{R}_v$ are the coordinates of the jth electron and vth nucleus, respectively, and N_v is the nucleus charge. Equation (10) extends beyond the framework of the traditional independent atom model (IAM) [94, 111], which considers the impact of structural changes but disregards the re-distribution of electron density resulting from bond formation and the effects of two-electron correlation.

The total diffraction signal in equation (10) comprises two parts. The diagonal terms $a = b$ correspond to scattering from the ground and excited states, while the off-diagonal

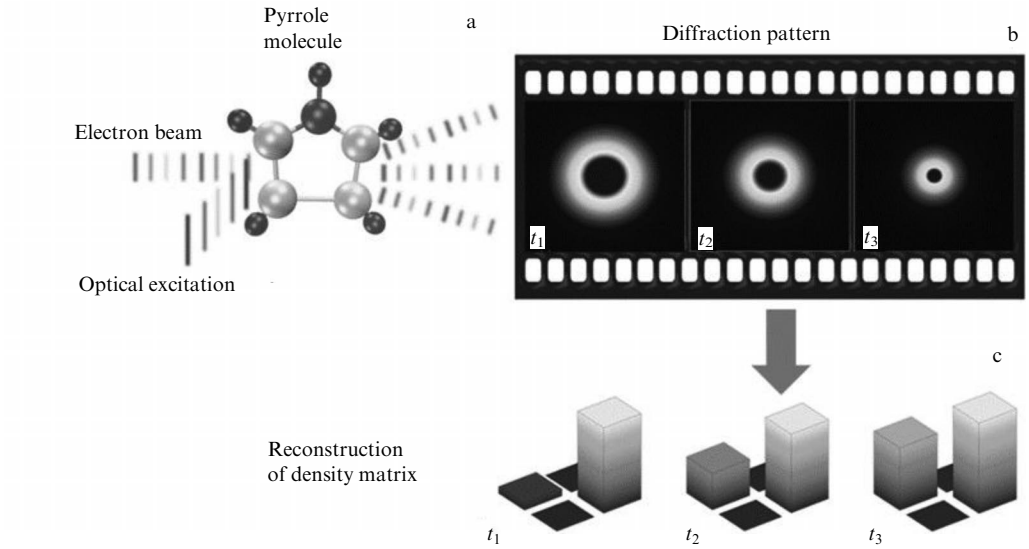

Figure 8. Schematic of quantum tomography of electron states using ultrafast electron diffraction. (a) Pyrrole molecule is excited by pumping laser and probed by ultrafast electron beam. (b) Diffraction patterns with temporal resolution for different time delays of pumping–probing. (c) Matrices of reduced density in basis of electron states are reconstructed from pattern of ultrafast electron diffraction with help of quantum tomography [107].

terms $a \neq b$ correspond to scattering from electron coherence [108]. The coherence term plays an important role when the nuclear wave packet passes through conical intersection regions, leading to changes in the diffraction signal [112]. However, the coherence term is much smaller than the diagonal terms in equation (10), and directly observing electron coherence through diffraction intensity remains difficult.

Time-resolved twisted X-ray diffraction is ultrafast nonresonant X-ray diffraction (XRD) using twisted X-ray beams carrying orbital angular momentum (OAM). The magnitude of OAM is unbounded and can take any integer value [113]. Using twisted X-ray beams with orbital angular momentum l allows the contributions of the diagonal terms to be compensated for, enabling the dynamics of electron coherence [113] to be observed directly. Changes in the diffraction intensity encode the information about nuclear and electron dynamics. In ultrafast electron diffraction of the pyridine molecule, the two components are naturally disentangled [110]. Electron state transitions correspond to low-angle signals, while nuclear structural dynamics correspond to signals at large angles. The low-angle signal dominates due to inelastic scattering [110, 114], arising from the effect of two-electron correlation due to Coulomb's repulsion and Pauli's exclusion [115, 116].

Compared to X-ray diffraction, the factor $1/s^2$ in $\hat{\sigma}_e$ of equation (13) considerably enhances the sensitivity of electron diffraction to the low-angle signals. If, for a given range of s, the approximation $I_{a,b}(\mathbf{R}, \mathbf{s}) \approx I_{a,b}(\mathbf{R}_0, \mathbf{s})$ is valid for a fixed nuclear geometry $\mathbf{R}_0$ when the amplitude of nuclear motion is small, then

$$I(\mathbf{s}, t) \approx \sum_{ab} \rho_{ab}(t)\, I_{a,b}(\mathbf{R}_0, \mathbf{s})\,.$$

In this case, the diffraction signal is directly linked to the reduced density matrix $\rho_{ab}(t)$, i.e., to the temporal evolution of populations and coherence, and $\rho_{ab}(t)$ can be recovered from ultrafast diffraction intensity, as shown in Fig. 8 [107] for a photoexcited pyrrole molecule.

In addition to ultrafast diffraction visualization, the QT of electron states and molecular orbitals can also be realized by spectroscopic visualization methods. For example, molecular QT in NH_3, using the time-resolved angular distribution of photoelectrons and kinetic energy spectrum, can fully characterize the dynamics of its electron state, population, and coherence [117]. The highest occupied molecular orbital (HOMO) of the N_2 molecule is tomographically reconstructed by detecting the generation spectra of higher harmonics for different angles of molecule orientation in a laser light field [118].

In this section, we presented the quantum tomography for molecular oscillations, rotations, and electron state dynamics. Combined with ultrafast diffraction visualization and spectroscopic visualization, QT provides a full quantum state description through these observables, enabling a quantum version of 'molecular movies.' A more challenging goal of QT for electron state dynamics is quantum process tomography (QPT), which involves reconstructing the process matrix and enables the prediction of time evolution beginning from an arbitrary (but known) initial state [119, 120]. QT of electron state dynamics is also a quite promising new direction, enabling one-electron and two-electron matrices of reduced density to be reconstructed. The latter includes information on the effect of electron correlation, which is of the utmost significance for strongly correlated systems.

6. Conclusions

In this review, we presented the main development stages in the field of detecting ultrafast structural dynamics using short electron pulses, beginning with a pioneering experiment conducted in Moscow in the 1980s. Successes in this field of science were fostered by the introduction of reliable solid-state pico-femtosecond lasers into scientific laboratories.

The development of UED/UEM has made it possible to study laser-induced processes over their natural spatial and temporal scales [121, 122]. The detection of structural dynamics using ultrashort electron pulses has even made it

possible to shoot molecular movies. High spatiotemporal resolution and a precise registration scheme were needed for this. When applied to the existing electron sources, such an ambitious task can currently only be achieved with the help of UED due to its higher sensitivity, particularly when studying complex biological molecules. In order to observe irreversible laser-induced processes, it is important to use dense multi-electron pulses. Pico-femtosecond temporal resolution is achieved by compression in a cell with an rf field or by transition to a relativistic regime, with each probing bunch containing up to several million electrons. Such approaches are now also beginning to be used in the UEM area.

A key advantage of the adapted transmission electron microscope is the wide spectrum of tasks it can assist with. In imaging mode, the effect of spatial irregularities in a sample on the structural dynamics can be studied. Time-resolved measurements of electron kinetic energy using the EELS method have two key applications: first, they enable the transition from 4D to 5D UEM for the study of laser-induced processes (in a spatiotemporal continuum, augmented by high resolution over energy), and second, they facilitate the development of attosecond (sub-femtosecond) microscopy.

To demonstrate the potential of time-resolved electron probing of ultrafast laser-induced processes, this review describes a series of important recent experiments in the field of UED/UEM. The review also presents femtosecond quantum tomography, which offers new opportunities for studying structural dynamics in a spatiotemporal continuum. We would like to conclude this review with the prophetic words of Louis de Broglie: ''In space-time everything which for each of us constitutes the past, the present and the future is given en bloc. ...''

S. A. A., B. N. M., D. G. P., and E. A. P. were supported by project FFUU-2025-0006 of the Institute of Spectroscopy of the RAS.

References

1. De Broglie L ''Recherches sur la théorie des quanta,'' Doctoral Dissertation (Paris: Masson, 1924); *Ann. Physique* **10** (3) 22 (1925) https://doi.org/10.1051/anphys/192510030022
2. Davisson C, Germer L H *Phys. Rev.* **30** 705 (1927)
3. Williams D B, Carter C B *Transmission Electron Microscopy. A Textbook for Materials Science* (New York: Springer, 2008)
4. Keller U *Nature* **424** 831 (2003)
5. Miller R J D *Annu. Rev. Phys. Chem.* **65** 583 (2014)
6. Zewail A H, Thomas J M *4D Electron Microscopy. Imaging in Space and Time* (London: Imperial College Press, 2010)
7. Chergui M, Zewail A H *Chem. Phys. Chem.* **10** 28 (2009)
8. Ischenko A A, Aseyev S A *Time Resolved Electron Diffraction: for Chemistry, Biology and Materials Science* (San Diego: Elsevier, 2014)
9. Ischenko A A, Weber P M, Miller R J D *Chem. Rev.* **117** 11066 (2017)
10. Ischenko A A et al. *Appl. Phys. B* **32** 161 (1983)
11. Siwick B J et al. *Science* **302** 1382 (2003)
12. Siwick B J et al. *J. Appl. Phys.* **92** 1643 (2002)
13. Muller D A *Nature Mater.* **8** 263 (2009)
14. Uhlemann St et al. *Phys. Rev. Lett.* **111** 046101 (2013)
15. Müller E W *Z. Phys.* **131** 136 (1951)
16. Binnig G, Quate C F, Gerber Ch *Phys. Rev. Lett.* **56** 930 (1986)
17. Campbell G H, McKeown J T, Santala M K, in *Springer Handbook of Microscopy* (Eds P W Hawkes, J C H Spence) (Cham: Springer, 2019) p. 455, https://doi.org/10.1007/978-3-030-00069-1_8
18. Aseyev S A et al. *Crystals* **10** (6) 452 (2020)
19. Filippetto D et al. *Rev. Mod. Phys.* **94** 045004 (2022)
20. Amini K, Rouzée A, Vrakking M J J (Eds) *Structural Dynamics with X-ray and Electron Scattering* (London: Royal Society of Chemistry, 2023) https://doi.org/10.1039/9781837671564
21. Balykin V I, Subbotin M V, Letokhov V S *Opt. Commun.* **129** 177 (1996)
22. Mironov B N et al. *J. Exp. Theor. Phys.* **106** 1007 (2008); *Zh. Eksp. Teor. Fiz.* **133** 1155 (2008)
23. van der Geer S B et al. *Microsc. Microanal.* **15** (4) 282 (2009)
24. de Raadt T C H, Franssen J G H, Luiten O J *Phys. Rev. Lett.* **130** 205001 (2023)
25. van Oudheusden T et al. *J. Appl. Phys.* **102** 093501 (2007)
26. van Oudheusden T et al. *Phys. Rev. Lett.* **105** 264801 (2010)
27. King W E et al. *J. Appl. Phys.* **97** 111101 (2005)
28. Xu C et al. *Nat. Commun.* **14** 1265 (2023)
29. Kieft E et al. *Struct. Dyn.* **2** 051101 (2015)
30. Andreev S V et al. *Quantum Electron.* **47** 116 (2017); *Kvantovaya Elektron.* **47** 116 (2017)
31. Aseyev S A et al. *Chem. Phys. Lett.* **797** 139599 (2022)
32. Du D X, Simjanoska M, Fitzpatrick A W P *J. Struct. Biol.* **215** 107941 (2023)
33. Shimojima T, Nakamura A, Ishizaka K *Microscopy* **72** (4) 287 (2023)
34. Shimojima T, Nakamura A, Ishizaka K *Rev. Sci. Instrum.* **94** 023705 (2023)
35. Makarov D N, Matveev V I *JETP Lett.* **101** 603 (2015); *Pis'ma Zh. Eksp. Teor. Fiz.* **101** 677 (2008)
36. Waldecker L et al. *Phys. Rev. X* **6** 021003 (2016)
37. Anisimov S I et al. *Sov. Phys. Tech. Phys.* **11** 945 (1967); *Zh. Eksp. Teor. Fiz.* **36** 1273 (1966)
38. Anisimov S I, Kapeliovich B L, Perel'man T L *Sov. Phys. JETP* **39** 375 (1974); *Zh. Eksp. Teor. Fiz.* **66** 776 (1974)
39. Sciaini G et al. *Nature* **458** 56 (2009)
40. Spivak G V, Saparin G V, Bykov M V *Sov. Phys. Usp.* **12** 756 (1970); *Usp. Fiz. Nauk* **99** 635 (1969)
41. Bostanjoglo O, Rosin Th *Opt. Acta Int. J. Opt.* **24** 657 (1977)
42. Jing Ch et al. *Ultramicroscopy* **207** 112829 (2019)
43. Barwick B, Flannigan D J, Zewail A H *Nature* **462** 902 (2009)
44. Talebi N *Near-Field-Mediated Photon–Electron Interactions* (Springer Ser. in Optical Sciences, Vol. 228) (Cham: Springer, 2019) https://doi.org/10.1007/978-3-030-33816-9
45. Kim Y-J et al. *Sci. Adv.* **9** eadd5375 (2023)
46. Pomarico E et al. *ACS Photon.* **5** 759 (2018)
47. Feist A et al. *Ultramicroscopy* **176** 63 (2017)
48. Houdellier F et al. *Ultramicroscopy* **186** 128 (2018)
49. Madan I et al. *Sci. Adv.* **5** eaav8358 (2019)
50. Bie Y-Q et al. *Ultramicroscopy* **230** 113389 (2021)
51. Zong A et al. *Nature* **620** 988 (2023)
52. Su Y et al. *Nano Lett.* **23** 10772 (2023)
53. González Vallejo I et al. *Phys. Rev. B* **97** 054302 (2018)
54. Durham D B et al. *Struct. Dyn.* **9** 064302 (2022)
55. Liu Y et al. *Nat. Commun.* **14** 2795 (2023)
56. Champenois E G et al. *Phys. Rev. Lett.* **131** 143001 (2023)
57. Nabben D et al. *Nature* **619** 63 (2023)
58. Mattes M, Volkov M, Baum P *Nat. Commun.* **15** 1743 (2024)
59. Yang Y et al. *Science* **383** 168 (2024)
60. Orville A M *Curr. Opin. Struct. Biol.* **65** 193 (2020)
61. Caffrey M, Cherezov V *Nat. Protoc.* **4** 706 (2009)
62. Cherezov V et al. *Science* **318** 1258 (2007)
63. Nogly P et al. *Science* **361** eaat0094 (2018) https://doi.org/10.1126/science.aat0094
64. Nass Kovacs G et al. *Nat. Commun.* **10** 3177 (2019)
65. Miller R J D et al. *Nat. Commun.* **11** 1240 (2020)
66. Francis W J C et al. *Struct. Dyn.* **11** 024301 (2024)
67. Nikbin E et al. *Microsc. Microanal.* **30** (Supplement_1) ozae044.936 (2024) https://doi.org/10.1093/mam/ozae044.936
68. Lvovsky A I, Raymer M G *Rev. Mod. Phys.* **81** 299 (2009)
69. Priebe K E et al. *Nature Photon.* **11** 793 (2017)
70. Smithey D T et al. *Phys. Rev. Lett.* **70** 1244 (1993)
71. Cai X et al. *Science* **338** 363 (2012)
72. Miquel C et al. *Nature* **418** 59 (2002)
73. Murch K W et al. *Nature* **502** 211 (2013)
74. Saglamyurek E et al. *Nature Photon.* **9** 83 (2015)

75. Pauli W, in *Quantentheorie* (Handbuch der Physik, Eds H Bethe et al.) (Berlin: Springer, 1933) p. 83, https://doi.org/10.1007/978-3-642-52619-0_2
76. Weigert S *Phys. Rev. A* **53** 2078 (1996)
77. Kim Y S, Noz M E *Phase Space Picture of Quantum Mechanics. Group Theoretical Approach* (World Scientific Lecture Notes in Physics, Vol. 40) (Singapore: World Scientific, 1991) https://doi.org/10.1142/1197
78. Li Z et al. *ACS Photon.* **7** 296 (2020)
79. Janicke U, Wilkens M *J. Mod. Opt.* **42** 2183 (1995)
80. Ischenko A A, Schaefer L, Ewbank J D *Proc. SPIE* **3516** 580 (1999); in *23rd Intern. Congress on High-Speed Photography and Photonics, 1998, Moscow, Russian Federation*
81. Leonhardt U, Raymer M G *Phys. Rev. Lett.* **76** 1985 (1996)
82. Leonhardt U et al. *Opt. Commun.* **127** 144 (1996)
83. Mouritzen A S, Mølmer K *Phys. Rev. A* **73** 042105 (2006)
84. Mouritzen A S, Mølmer K *J. Chem. Phys.* **124** 244311 (2006)
85. Opatrný T, Welsch D-G, Vogel W *Phys. Rev. A* **56** 1788 (1997)
86. Branderhorst M P A et al. *J. Phys. B* **41** 074004 (2008)
87. Margulis B et al. *Science* **380** 77 (2023)
88. Laurell H et al. *Phys. Rev. Research* **4** 033220 (2022)
89. Dunn T J, Walmsley I A, Mukamel S *Phys. Rev. Lett.* **74** 884 (1995)
90. Skovsen E et al. *Phys. Rev. Lett.* **91** 090406 (2003)
91. Kurtsiefer Ch, Pfau T, Mlynek J *Nature* **386** 150 (1997)
92. Stankus B et al. *Nat. Chem.* **11** 716 (2019)
93. Starodub D et al. *Nat. Commun.* **3** 1276 (2012)
94. Yang J et al. *Science* **361** 64 (2018)
95. Wolf T J A et al. *Nat. Chem.* **11** 504 (2019)
96. Eichberger M et al. *Nature* **468** 799 (2010)
97. Mehrabi P et al. *Science* **365** 1167 (2019)
98. Chapman H N et al. *Nature* **470** 73 (2011)
99. Seibert M M et al. *Nature* **470** 78 (2011)
100. Chen C-C et al. *Phys. Rev. B* **76** 064113 (2007)
101. Fienup J R *Appl. Opt.* **21** 2758 (1982)
102. Marchesini S *Rev. Sci. Instrum.* **78** 011301 (2007)
103. Zhang M et al. *Nat. Commun.* **12** 5441 (2021)
104. Ewbank J D, Schäfer L, Ischenko A A *J. Mol. Struct.* **524** 1 (2000)
105. Ischenko A A, Weber P M, Miller R J D *Russ. Chem. Rev.* **86** 1173 (2017); *Usp. Khim.* **86** 1173 (2017)
106. Ischenko A A *Phys. Res. Int.* **2013** 236743 (2013)
107. Jiang J et al. *J. Chem. Phys.* **160** 104101 (2024)
108. Kowalewski M, Bennett K, Mukamel S *Struct. Dyn.* **4** 054101 (2017)
109. Zhang M et al. *J. Phys. Chem. Lett.* **13** 1668 (2022)
110. Yang J et al. *Science* **368** 885 (2020)
111. Santra R *J. Phys. B* **42** 169801 (2009)
112. Keefer D et al. *Proc. Natl. Acad. Sci. USA* **118** e2022037118 (2021)
113. Yong H et al. *Phys. Rev. Lett.* **129** 103001 (2022)
114. Mu X et al. *Ultrafast Sci.* **3** 0015 (2023)
115. Iijima T, Bonham R A, Ando T *J. Phys. Chem.* **67** 1472 (1963)
116. Bartell L S, Gavin R M *J. Am. Chem. Soc.* **86** 3493 (1964)
117. Morrigan L et al. *Phys. Rev. Lett.* **131** 193001 (2023)
118. Itatani J et al. *Nature* **432** 867 (2004)
119. Yuen-Zhou J, Aspuru-Guzik A *J. Chem. Phys.* **134** 134505 (2011)
120. Yuen-Zhou J et al. *Proc. Natl. Acad. Sci. USA* **108** 17615 (2011)
121. Aseyev S A, Weber P M, Ischenko A A *J. Anal. Sci. Meth. Instrum.* **3** 30 (2013) https://doi.org/10.4236/jasmi.2013.31005
122. Ischenko A A et al. *Fine Chem. Technol.* **12** (1) 5 (2017) https://doi.org/10.32362/2410-6593-2017-12-1-5-25